29th International Congress on Sound and Vibration
The annual congress of the International Institute of Acoustics and Vibration (IIAV)
9–13 July 2023
ICSV29

MODELLING OF ACOUSTIC INSTABILITIES IN A FLOW DUCT WITH THE GREEN'S FUNCTION APPROACH

Jiasen Wei, Jan O. Pralits, and Alessandro Bottaro
Department of Civil, Chemical and Environmental Engineering, University of Genoa, 16145 Genoa, Italy
e-mail: jiasen.wei@edu.unige.it
Sadaf Arabi and Maria Heckl
School of Physical and Chemical Sciences, Keele University, ST5 5BG Staffordshire, United Kingdom
email: s.arabi@keele.ac.uk

Thermoacoustic instabilities and aeroacoustic instabilities are due to feedback between acoustic field and unsteady heat release or unsteady flow fluctuations. The Green's function approach is a robust and fast analytical tool to study self-excited acoustic oscillations in such systems. If the mean flow is included, the reciprocity of the Green's function is lost. This work aims to extend the framework of the Green's function approach for modelling thermoacoustic instabilities in the presence of mean flow by demonstrating the symmetry of the Green's function. The framework is applied to a one-dimensional combustion system with a compact flame whose heat release rate is described by a generalized nonlinear time-lag law. Our extended Green's function approach is able to capture the effect of mean flow on the instabilities as well as the nonlinear dynamics of the system, showing that increasing the mean flow can expand the stable region of the stability map.
Keywords: Thermoacoustic instability, Green's function, Nonlinear dynamics, Mean flow effects

1. Introduction

Self-excited oscillations in thermoacoustic and aeroacoustic systems can cause damage to equipment structures. The problem of thermoacoustic instability arose with the invention of premixed combustion and hydrogen combustion for NOx emission reduction [1, 2, 3]. Aeroacoustic whistling is observed in confined geometries and can be mitigated by using devices such as mufflers, perforated plates, and Helmholtz resonators. Compared to experiments and CFD investigations, analytical models can capture major properties of these phenomena and significantly reduce computational costs, such as low-order network modeling [4, 5] and the Galerkin technique [6]. The Green's function is a fast and robust tool widely used in the study of wave propagation. It can express acoustic disturbances in the form of an integral equation. In an unbounded space, the Green's function is called the free-space Green's function, of which the analytical solution is known. In a confined space, the Green's function satisfying certain boundary conditions is called exact Green's function or tailored Green's function. [7] gave a summary of the tailored Green's function framework in the study of aerodynamics and thermoacoustic instabilities. However, most investigations using Green's function approach adopted the zero-Mach assumption, which limits the versatility of the model.

This work aims to extend the tailored Green's function approach to model the thermoacoustic instabilities in a horizontal Rijke tube in the presence of a steady and uniform mean flow. We first illustrate

a one-dimensional prototype thermoacoustic system. Second, we demonstrate the process to obtain the integral governing equation of acoustic velocity fluctuation and the solution of the tailored Green's function. We also calculate the linear stability for given initial conditions and heat source positions. Then, some results of the nonlinear dynamics, hysteresis behavior, and the mean flow effect are discussed. Finally, conclusions are given.

2. Problem description

The present work investigated a thermoacoustic system consisting of a one-dimensional horizontal tube with a steady and uniform mean flow in the axial direction, and an unsteady heat source located at x_q. The acoustic field is governed by an inhomogeneous convected wave equation:

$$\mathcal{L}\phi = \frac{\partial^2\phi}{\partial t^2} + 2\bar{u}\frac{\partial^2\phi}{\partial t\partial x} + (\bar{u}^2 - c^2)\frac{\partial^2\phi}{\partial x^2} = -\frac{\gamma - 1}{\bar{\rho}}q, \tag{1}$$

where $\mathcal{L}$ is the linear operator of ϕ in the convected wave equation, ϕ is the fluctuation of the velocity potential, $\bar{u}$ is the mean flow velocity, $\bar{\rho}$ is the mean density of the fluid in the duct, c is the speed of sound, and γ is the specific heat capacity ratio. $q(x,t)$ is the volumetric unsteady heat release rate generated by the heat source. The heat source is assumed to be acoustically compact, $q(x,t) = q(t)\delta(x - x_q)$, and we used a generalized amplitude-dependent heat release law reported in [8]:

$$q(t) = \bar{\rho}K[n_1 u_q(t - \tau_q) - n_0 u_q(t)] \tag{2}$$

with K the heat power per unit mass flow. The coupling coefficients n_0 and n_1, and time delay τ_q are functions of the dimensionless velocity fluctuation amplitude $(A/\bar{u})$.

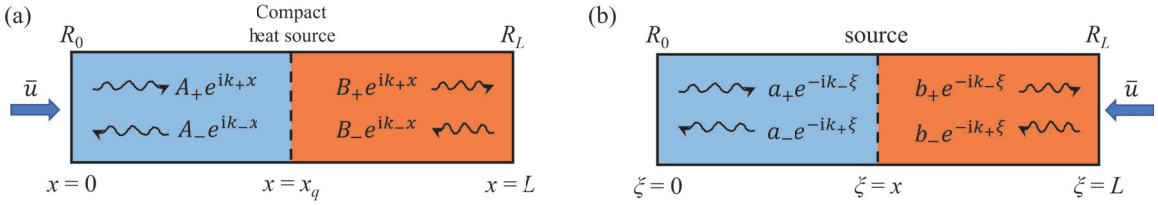

Figure 1: (a) Sketch of ϕ propagating in a horizontal duct in the presence of steady mean flow $\bar{u}$.
(b) Sketch of G propagating in a horizontal duct with reversed steady mean flow $\bar{u}$.

Fig. 1(a) shows a schematic view of the acoustic propagation in the system. The length of the duct is L, and an acoustically compact heat source is located at $x = x_q$. The duct has arbitrary acoustic boundary conditions at the inlet and outlet, represented by the reflection coefficients R_0 and R_L, respectively. An initial perturbation is assigned to the system at the heat source position to observe the stability behavior. Therefore, the initial conditions are given as:

$$\phi(x, t = 0) = \varphi_0\delta(x - x_q) \quad \text{and} \quad \left(\frac{\partial}{\partial t} + \bar{u}\frac{\partial}{\partial x}\right)\phi(x, t = 0) = \varphi_0'\delta(x - x_q) \tag{3}$$

where φ_0 and φ_0' are constants. The condition for the material derivative of the velocity potential defines the initial pressure field.

3. The Green's function approach

3.1 The integral governing equation

The Green's function approach exploits Lagrange's identity to develop an integral equation for ϕ. First we define the inner product of two arbitrary functions $w(\xi,\tau)$ and $v(\xi,\tau)$,

$$\langle w(\xi,\tau), v(\xi,\tau)\rangle = \int_{\xi}\int_{\tau} w(\xi,\tau)v(\xi,\tau)\mathrm{d}\tau\mathrm{d}\xi, \tag{4}$$

where ξ and τ are "active" spatial and time variables, integrated over the respective domains of interest. We introduce an arbitrary test function G and apply integration by parts to the inner product of G and Eq. (1). This results in what is sometimes known as Lagrange's identity:

$$\langle \mathcal{L}\phi, G\rangle = \langle \phi, \mathcal{L}^* G\rangle + \text{boundary terms}. \tag{5}$$

$\mathcal{L}^*$ above is the adjoint operator associated with $\mathcal{L}$. G is the solution of

$$\mathcal{L}^* G = \frac{\partial^2 G}{\partial \tau^2} + 2\bar{u}\frac{\partial^2 G}{\partial \tau \partial \xi} + (\bar{u}^2 - c^2)\frac{\partial^2 G}{\partial \xi^2} = \delta(\xi - x)\delta(\tau - t), \tag{6}$$

G is chosen to satisfy the same acoustic boundary conditions as ϕ at the ends of the duct

$$R_0 = \frac{a_+}{a_-} = \frac{A_+}{A_-}, \quad \text{at } \xi = 0; \qquad R_L = \frac{b_-\mathrm{e}^{-ik_+L}}{b_+\mathrm{e}^{-\mathrm{i}k_-L}} = \frac{B_-\mathrm{e}^{ik_-L}}{B_+\mathrm{e}^{\mathrm{i}k_+L}}, \quad \text{at } \xi = L. \tag{7}$$

where A_+, A_-, B_+, B_- are the wave amplitudes of ϕ illustracted in Fig. 1(a); a_+, a_-, b_+, b_- are the wave amplitudes of G. $k_+ = \omega/(\bar{u}+c)$ and $k_- = \omega/(\bar{u}-c)$ are the wave numbers. G is subject to terminal conditions at the final time $\tau = \boldsymbol{T}$:

$$G(\xi, x, \boldsymbol{T}, t) = 0, \qquad \frac{\partial G}{\partial \tau}(\xi, x, \boldsymbol{T}, t) + \bar{u}\frac{\partial G}{\partial \xi}(\xi, x, \boldsymbol{T}, t) = 0. \tag{8}$$

The test function G is called the adjoint Green's function [9]. G can be interpreted as an impulse response in the given geometry with the mean flow direction reversed, as sketched in Fig. 1(b). This is what Howe called the "reverse flow theorem" [10]. It comes from the property sometimes called the symmetry of Green's function, i.e.

$$G(x, x^*, t, t^*) = g(x^*, x, t^*, t). \tag{9}$$

The direct-source Green's function [9], denoted as g, is obtained by applying the inner product and Lagrange's identity, $\langle \mathcal{L}g, G\rangle = \langle g, \mathcal{L}^* G\rangle$. Eq. 9 describes the relationship between the adjoint Green's function and the direct-source Green's function. Its detailed proof can be found in [11, 12].

With Eqns. (5)-(8), the boundary terms related to the boundary conditions can be eliminated. Eventually, by definition of velocity potential, the velocity fluctuation at the compact source position x_q is,

$$\begin{aligned} u_q(t) =& \frac{\partial \phi}{\partial x}\bigg|_{x=x_q} = -\frac{\gamma - 1}{\bar{\rho}}\int_{\tau=0}^{t} \frac{\partial G(x_q, x, \tau, t)}{\partial x}\bigg|_{x=x_q} q(\tau)\mathrm{d}\tau + \\ & - \varphi_0 \frac{\partial}{\partial x}\left[\frac{\partial G}{\partial \tau}(x_q, x, 0, t) + \bar{u}\frac{\partial G}{\partial \xi}(x_q, x, 0, t)\right]\bigg|_{x=x_q} + \varphi_0' \frac{\partial G(x_q, x, 0, t)}{\partial x}\bigg|_{x=x_q}. \end{aligned} \tag{10}$$

As long as the solution of G is known, we can obtain the time history of u_q. With the wave-form assumption, we can calculate G analytically using a similar approach in [7]. The solution of the G is a superposition of modes with modal amplitudes g_n and modal frequencies ω_n:

$$G(\xi, x, \tau, t) = \mathrm{Re} \sum_{n=1}^{\infty} \hat{g}_n(\xi, x) \mathrm{e}^{\mathrm{i}\omega_n(\tau - t)}, \tag{11}$$

where Re denotes the real part and

$$\hat{g}_n(\xi, x) = -\frac{\psi(x, \omega_n)}{c\,\omega_n F'(\omega_n)} \begin{cases} \beta(x, \omega_n)\alpha(\xi, \omega_n) & \text{for } \xi < x \\ \alpha(x, \omega_n)\beta(\xi, \omega_n) & \text{for } \xi > x \end{cases}, \tag{12}$$

with

$$\psi(x, \omega) = \mathrm{e}^{\mathrm{i}(k_+ + k_-)x}, \tag{13a}$$
$$\alpha(\xi, \omega) = R_0 \mathrm{e}^{-\mathrm{i}k_-\xi} + \mathrm{e}^{-\mathrm{i}k_+\xi}, \tag{13b}$$
$$\beta(\xi, \omega) = \mathrm{e}^{-\mathrm{i}k_-\xi} + R_L \mathrm{e}^{\mathrm{i}(k_+ - k_-)L} \mathrm{e}^{-\mathrm{i}k_+\xi}, \tag{13c}$$
$$F(\omega) = 1 - R_0 R_L \mathrm{e}^{\mathrm{i}(k_+ - k_-)L}. \tag{13d}$$

ω_n, the natural frequency of the n-th mode, is the solution of the characteristic equation $F(\omega) = 0$. $F'(\omega)$ in Eq. (12) represents the first-derivative of $F(\omega)$ with respect to ω.

3.2 Modal analysis

The Green's function contains information on the eigenmodes of the system without the heat source. The signal of velocity fluctuation u_q is the sum of eigenmodes of the system with thermoacoustic feedback including the heat source. The integral equation (Eq. 10) relates the two parts together. The stability of the system with the heat source can be obtained by modal analysis. The velocity fluctuations can be expressed as a superposition of eigenmodes with complex frequencies Ω_m and complex amplitudes u_m,

$$u_q(t) = \sum_{m=1}^{\infty} \left(u_m \mathrm{e}^{-\mathrm{i}\Omega_m t} + u_m^* \mathrm{e}^{\mathrm{i}\Omega_m^* t} \right), \tag{14}$$

where the superscript $*$ denotes the complex conjugate. By substituting Eqns. (2), (11), and (14), into Eq. (10), and after some mathematical manipulations (details are ready to be submitted to a journal), we obtain two equations for the two unknowns u_m and Ω_m,

$$\left(n_0 - n_1 \mathrm{e}^{\mathrm{i}\Omega_m \tau_q}\right) \sum_{n=1}^{\infty} \left[\frac{G_n}{-i(\Omega_m - \omega_n)} + \frac{G_n^*}{-\mathrm{i}(\Omega_m + \omega_n^*)} \right] = \frac{2}{(\gamma - 1)K} \tag{15a}$$

$$\sum_{m=1}^{\infty} \left[\frac{-u_m \left(n_0 - n_1 \mathrm{e}^{\mathrm{i}\Omega_m \tau_q}\right)}{-\mathrm{i}(\Omega_m - \omega_n)} + \frac{-u_m^* \left(n_0 - n_1 \mathrm{e}^{-\mathrm{i}\Omega_m^* \tau_q}\right)}{\mathrm{i}(\Omega_m^* + \omega_n)} \right] = \frac{\mathrm{i}\omega_n \varphi_0 - \varphi_0'}{(\gamma - 1)K} + \frac{\varphi_0 \bar{u} \alpha'}{(\gamma - 1)K\alpha}, \tag{15b}$$

and their complex conjugates, where $G_n = \left.\dfrac{\partial \hat{g}_n(x_q, x, \omega_n)}{\partial x}\right|_{x=x_q}$ and $\alpha' = \left.\dfrac{\partial \alpha(x, \omega_n)}{\partial x}\right|_{x=x_q}$. The real part of Ω_m gives the angular frequency of the oscillation of velocity fluctuations. The imaginary part of Ω_m gives the growth rate of the velocity fluctuations in the presence of thermoacoustic feedback.

4. Results and discussions

In this section, we show the stability behavior of the first acoustic eigenmode in a horizontal Rijke tube. The length of the Rijke tube is $L = 2$ m. The mean temperature, $\bar{T} = 304$ K, is uniform along the tube, and the corresponding speed of sound is $c = 350$ m s^{-1}. The heater power is $K = 3\times10^5$ W s kg^{-1}. The open ends employ the reflection coefficients $R_0 = -1$ and $R_L = -1$.

4.1 Validation

Validation against a wave-based network modelling approach is shown in Fig 2. We calculated the

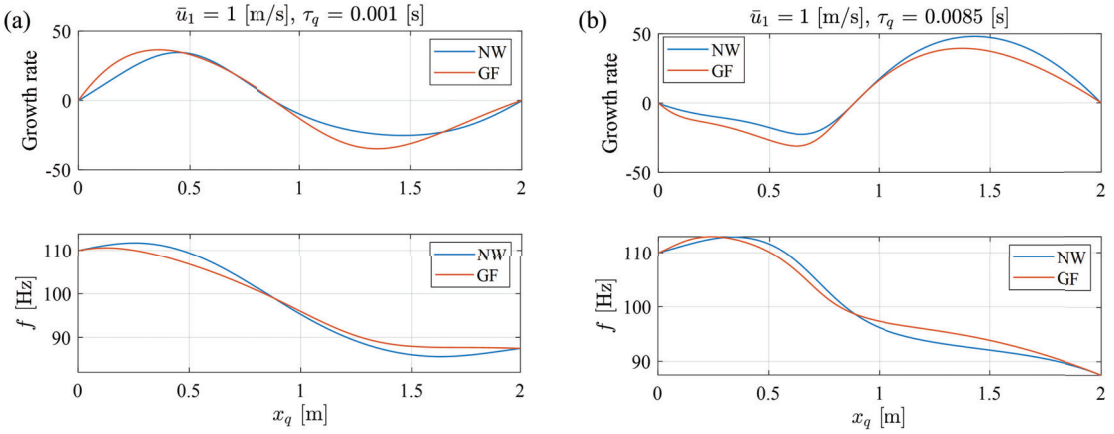

Figure 2: Dependence of linear stability on the heat source position. A comparison of eigenvalues computed with Green's function approach (GF) and network modeling approach (NW). $\bar{u}_1 = 1$ m s^{-1}, $A/\bar{u} = 0$, $n_0 = 0$, $n_1 = 1$. (a) $\tau_q = 0.001$ s; (b) $\tau_q = 0.0085$ s.

linear stability of a horizontal Rijke tube system at different heat source positions. The inlet mean flow velocity is set to be $\bar{u}_1 = 1$ m s^{-1}. The temperature upstream of the heat source is $\bar{T}_1 = 304$ K, and the temperature downstream of the heat source is $\bar{T}_2 = 484$ K, giving the respective speed of sound $c_1 = 350$ m s^{-1} and $c_2 = 440$ m s^{-1}. The wave-based network modelling approach is adopted from [5] p.756-757, example 4. The eigenvalues calculated with the Green's function approach show good agreement with the results of the network modelling approach.

Another validation is carried out by comparing the stability map of a zero-Mach number case with the stability map created with Green's function of [7], as shown in Fig. 3. Stability maps are created based on modal analysis calculations to show the dependence of growth rate on $\dfrac{A}{\bar{u}}$ and x_q. It is observed that under the zero-Mach condition, the two stability maps coincide. Thus, when setting the mean flow to zero, our model coincides with the Green's function model of the self-adjoint problem.

4.2 Dependence on heat source position

The stability of the system and hysteresis phenomena that occur when changing the heat source location are discussed in this section. Figure 4(a) shows the stability map when Mach number $Ma = \bar{u}/c = 0.0004$, i.e. the mean flow velocity is $\bar{u} = 0.141$ m s^{-1}. It shows that when the heat source is located on the upstream half of the duct, the system is linearly unstable. This is a well-known property of

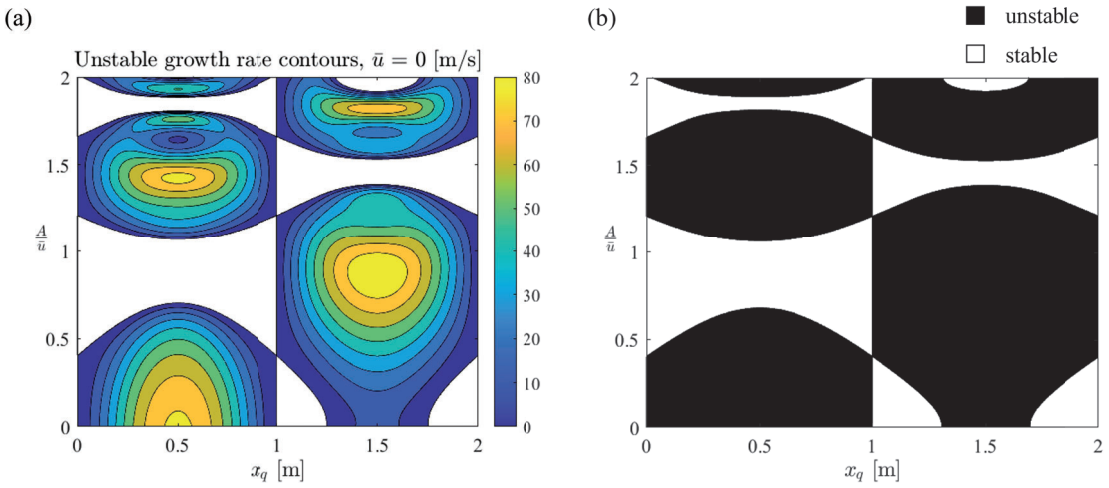

Figure 3: Stability maps of a uniform Rijke tube in the absence of mean flow, (a) computed with the present G solution; (b) computed with G solution reported in [7].

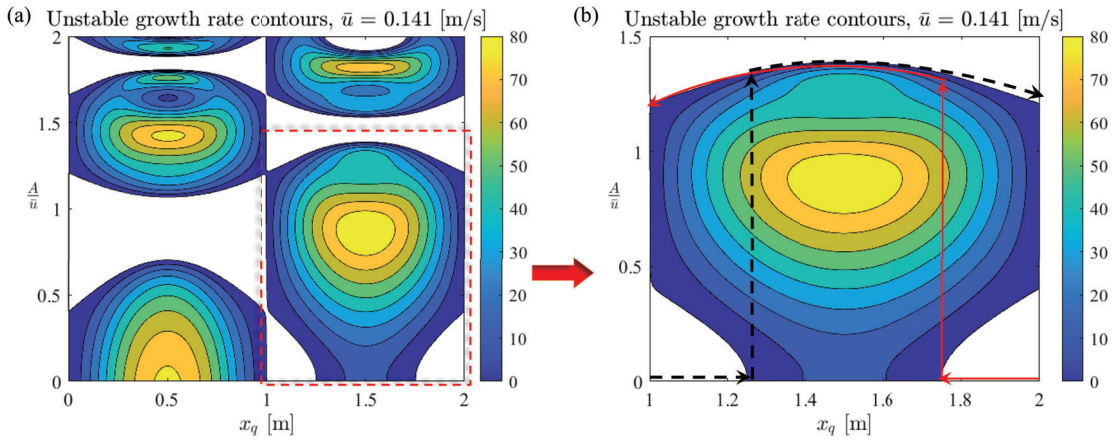

Figure 4: Stability maps of a uniform Rijke tube, $Ma = 0.0004$.

a Rijke tube when the time lag is in the range of $0 < \tau_q < \mathcal{T}_1/2$ with $\mathcal{T}_1$ the first-mode oscillation period of the acoustic wave [13]. In the present case, the time lag is slightly smaller than $\mathcal{T}_1/2$.

At the downstream half of the tube, we observe two hysteresis zones. An enlarged view is shown in Figure 4(b). Starting from $x_q = 1$ m and with a small initial condition assigned to the system, we observe that as the heat source is moved downstream, the system behaves following the path marked by the black dashed curve. The system stays linearly stable until it reaches $x_q = 1.25$ m. Then, the system is unstable and the amplitude of u_q grows until it oscillates as a limit cycle. This is a subcritical Hopf bifurcation and the region between $x_q = 1.00 \sim 1.25$ m is a hysteresis zone. The stability of the system in the hysteresis zone depends on the initial excitation amplitude. Another subcritical bifurcation can be observed if we follow a reverse path, i.e. moving the heat source upstream starting from the outlet. The stability behavior of the system is marked by the red solid curve and a second hysteresis zone is found in the range 1.75 m $\leq x_q \leq 2.00$ m. Our prediction qualitatively agrees with the experiment results by [14]. They have found subcritical Hopf bifurcations appearing when moving the heat source from the

duct inlet to the outlet and during the reverse path, respectively. However, the width of the hysteresis zone is not the same, and the fold point is not clear in our stability maps. The differences are due to several possible reasons: The heat release model used here is a generalized model and does not describe precisely the mesh electric heater used in the experiments. Furthermore, our stability map only follows the first eigenmode of the system. Although low-frequency modes usually have a larger contribution to acoustic energy, the measured oscillations observed in experiments are a sum of all eigenmodes.

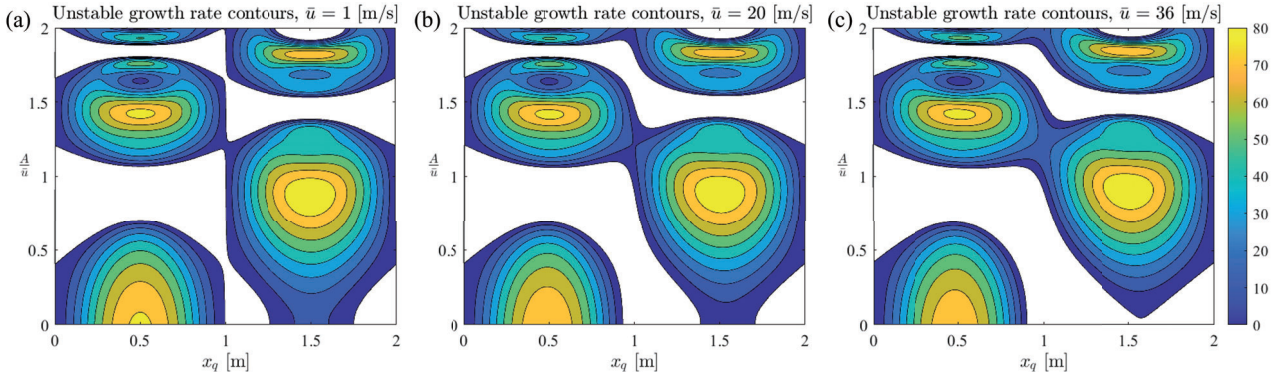

Figure 5: Stability maps of a uniform Rijke tube when the mean flow velocity are (a) $\bar{u} = 1$ m s^{-1}; (b) $\bar{u} = 20$ m s^{-1}; (c) $\bar{u} = 36$ m s^{-1}.

4.3 Dependence on mean flow velocity

Figure 5 shows the stability maps of a uniform Rijke tube in the presence of different mean flow velocities. Increasing the mean flow velocity reduces both linearly unstable regions in the duct's upstream and downstream half. In the unstable region, the growth rate is moderately reduced for larger $\bar{u}$. This indicates that increasing the mean flow velocity has a stabilizing effect on the system. The first hysteresis zone is pushed downstream and a larger initial excitation amplitude is required for the system to be unstable. For the present problem, the unstable zone in the downstream half as well as the hysteresis zones will disappear when the mean flow velocity is larger than $\bar{u} = 36$ m s^{-1}. Experiments to study the effect of mass flow rate on hysteresis behavior have also been conducted by [14]. It is reported that for high mass flow rates in the investigated range (corresponding to $Ma = 0.00036 \sim 0.00067$, approximately), the hysteresis zone will be narrower but there exists a definite subcritical bifurcation. According to our model's prediction, the subcritical bifurcation exists until the Mach number reaches about $Ma = 0.1$.

5. Conclusions

This work has described a Green's-function-based framework to study the dynamics of self-excited acoustic oscillations in a one-dimensional thermoacoustic system: a uniform Rijke tube in the presence of a steady mean flow. Our model is able to predict the stability of the system and the nonlinear dynamics of the oscillations, such as limit cycles and subcritical bifurcations. The model can capture the hysteretic behavior observed in experiments when changing the heat source positions in the duct. The effect of the mean flow velocity on the system stability is discussed. It is found that increasing the mean flow can stabilize the system, narrow the unstable region in the stability map, and push the hysteresis zone downstream. The hysteresis phenomena disappear when the Mach number reaches $Ma = 0.1$.

Acknowledgement

This work is part of the Marie Skłodowska-Curie Innovative Training Network *Pollution Know-How and Abatement* (POLKA). We gratefully acknowledge the financial support from the European Union's Horizon 2020 research and innovation programme under the Marie Skłodowska-Curie grant agreement No. 813367.

REFERENCES

1. Lieuwen, T. C. and Yang, V., *Combustion instabilities in gas turbine engines: operational experience, fundamental mechanisms, and modeling*, American Institute of Aeronautics and Astronautics (2005).

2. Candel, S. Combustion dynamics and control: Progress and challenges, *Proceedings of the Combustion Institute*, **29** (1), 1–28, (2002).

3. Crocco, L. and Cheng, S.-I., *Theory of combustion instability in liquid propellant rocket motors*, Princeton Univ, NJ (1956).

4. Evesque, S. and Polifke, W. Low-order acoustic modelling for annular combustors: validation and inclusion of modal coupling, *Turbo Expo: Power for Land, Sea, and Air*, vol. 36061, pp. 321–331, (2002).

5. Dowling, A. P. and Stow, S. R. Acoustic analysis of gas turbine combustors, *Journal of Propulsion and Power*, **19** (5), 751–764, (2003).

6. Balasubramanian, K. and Sujith, R. I. Thermoacoustic instability in a Rijke tube: Non-normality and nonlinearity, *Physics of Fluids*, **20** (4), 044103, (2008).

7. Heckl, M. A., Gopinathan, S. M. and Surendran, A. A unified framework for acoustic instabilities based on the tailored Green's function, *Journal of Sound and Vibration*, **541**, 117279, (2022).

8. Bigongiari, A. and Heckl, M. A. A Green's function approach to the rapid prediction of thermoacoustic instabilities in combustors, *Journal of Fluid Mechanics*, **798**, 970–996, (2016).

9. Tam, C. K. W. and Auriault, L. Mean flow refraction effects on sound radiated from localized sources in a jet, *Journal of Fluid Mechanics*, **370**, 149–174, (1998).

10. Howe, M. The generation of sound by aerodynamic sources in an inhomogeneous steady flow, *Journal of Fluid Mechanics*, **67** (3), 597–610, (1975).

11. Morfey, C. L., Powles, C. J. and Wright, M. C. M. Green's functions in computational aeroacoustics, *International Journal of Aeroacoustics*, **10** (2-3), 117–159, (2011).

12. Greenberg, M. D., *Foundations of Applied Mathematics*, Prentice-Hall, Inc., Englewood Cliffs, N.J. (1978).

13. Dowling, A. P., Ffowcs-Williams, J. E. and Sevik, M. M. Sound and Sources of Sound, *Journal of Vibration, Acoustics, Stress, and Reliability in Design*, **106** (3), 320–320, (1984).

14. Gopalakrishnan, E. A. and Sujith, R. I. Influence of system parameters on the hysteresis characteristics of a horizontal Rijke tube, *International Journal of Spray and Combustion Dynamics*, **6** (3), 293–316, (2014).